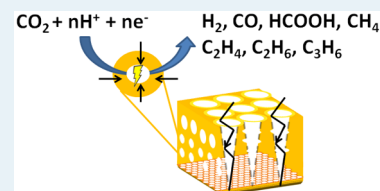# Electrochemical Reduction of CO_2 at Copper Nanofoams

Sujat Sen,[†] Dan Liu,[†] and G. Tayhas R. Palmore*[,†,‡]

[†]Department of Chemistry and [‡]School of Engineering, Brown University, Providence, Rhode Island 02912, United States

S *Supporting Information*

ABSTRACT: We report the electrochemical reduction of CO_2 at copper foams with hierarchical porosity. We show that both the distribution of products formed from this reaction and their faradaic efficiencies differ significantly from those obtained at smooth electropolished copper electrodes. We attribute these differences to be due to high surface roughness, hierarchical porosity, and confinement of reactive species. We provide preliminary evidence in support of these claims.

$CO_2 + nH^+ + ne^-$ → H_2, CO, HCOOH, CH_4 C_2H_4, C_2H_6, C_3H_6

KEYWORDS: CO_2 reduction, copper foam, formic acid, nanoporous, confinement effects

Electrochemical reduction of CO_2 has been investigated at a variety of metallic electrodes, and a number of reports and reviews have been published on this subject.[1−9] Among the metals studied, copper generates significant quantities of hydrocarbons such as methane and ethylene in aqueous media.[7] Hori et al.[3,10−14] conducted extensive studies on the electrochemical reduction of CO_2 and CO at copper electrodes and concluded that the product distribution reflected a sensitivity of adsorbed hydrogen species to the underlying structure of the copper electrode and that "surface roughening likely introduced surface defects such as steps and vacancies that are favorable for reaction of adsorbed hydrogen atoms".[12,13] Several other groups have reported on the electrochemical reduction of CO_2 at copper electrodes in aqueous and nonaqueous media with various supporting electrolytes.[7,15−17] Nanoparticulate and nanoporous electrode surfaces of copper and other metals have been used to study effects of particle size and porosity.[18−20] Norskov et al.[18] studied copper electrodes with three different morphologies (electropolished, sputter coated, and nanoparticle coated) for their selectivity toward CO_2 reduction. They found that the latter two morphologies were more selective toward hydrocarbon generation and attributed this effect to the greater abundance of uncoordinated sites.[18] DFT calculations further suggested that these sites are the most likely sites involved in CO_2 activation and reduction. Other computational studies have been performed to explain the catalytic behavior and selectivity of copper toward CO_2 reduction.[21−24]

Recent work[23] that describes a novel approach to the fabrication of metal foams with hierarchical porosity provides an excellent opportunity for testing the effect of three-dimensional nanostructured metal surfaces and their corresponding cavities on the products produced during the electrochemical reduction of CO_2. In this paper, we show that the electrochemical reduction of CO_2 at copper foams yields formic acid at a lower onset potential with faradaic efficiencies that are 10−20% higher than other reported values. In comparison to smooth copper electrodes, the faradaic efficiencies of CO, methane, and ethylene are reduced

significantly, whereas C2 and C3 products such as ethane and propylene are produced in small but detectable quantities. Although ethane has been observed at very low yields,[18] propylene has not been observed previously at copper electrodes. The presence of ethane and propylene suggests that copper foams provide both the nanostructured surfaces and cavities that facilitate the reaction between adsorbed CO_2 and hydrogen species to generate higher-order hydrocarbons during the electrochemical reduction of CO_2.

Three-dimensional foams of copper were electrodeposited onto mechanically polished copper substrates using a reported procedure.[25] This procedure is simple to perform and results in an electrode with hierarchical porosity. Evolution of hydrogen gas at an electrode surface is significant during the electro-deposition of copper when a high current density is maintained (typically >0.5 A/cm²). The evolution of hydrogen gas impedes electrodeposition of copper directly onto the cathode by temporarily preventing contact between the copper cathode and the electrolyte that contains copper sulfate. Eventually, a thin film of electrolyte surrounding a H_2 bubble comes into contact with the cathode, which completes the electrochemical circuit and allows for the electrodeposition of copper. The resulting foam is a connected network of copper pores templated by H_2 bubbles. Shown in Figure 1 are typical SEM images of copper foams electrodeposited for different amounts of time. Copper foams appear reddish when freshly electro-deposited (inset) but gradually dull with exposure to air as the copper is oxidized. Nanoscale dendritic structures protrude from the walls of the pores (Figure 1f). The pore diameter (20−50 μm) can be controlled by electrodeposition parameters such as concentration of copper salts, pH, and deposition time.[25]

Shown in Figure 2a is the X-ray diffractogram (XRD) of electrodeposited copper foam on an aluminum substrate, which reveals that copper foams have face-centered cubic structure
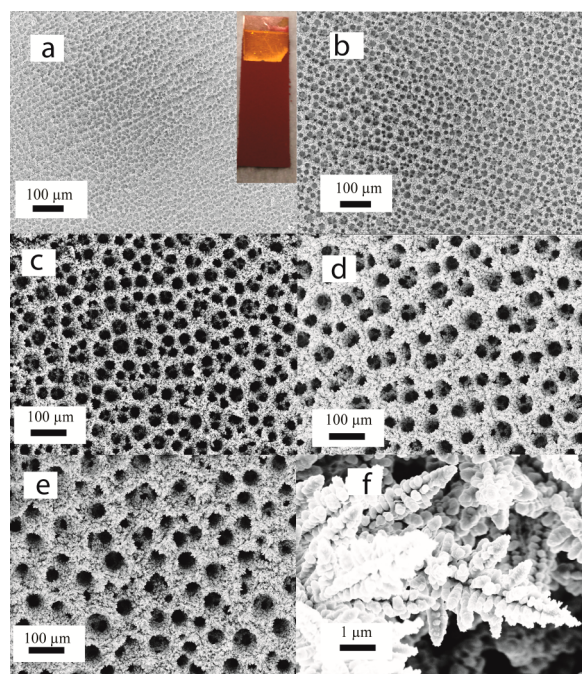
Figure 1. SEM images of electrodeposited copper foams on a copper substrate for (a) 5s; (b) 10s; (c) 15s; (d) 30s; and (e) 60s; (f) nanostructure of the electrodeposited foams. Inset of (a) is a photo of a copper electrode immediately after electrodeposition of the copper foam.
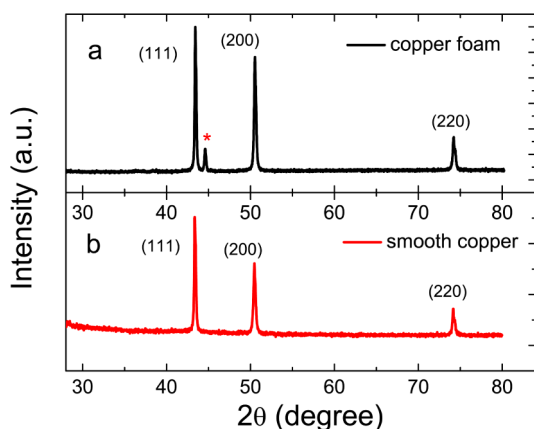

Figure 2. (a) XRD patterns of an Al substrate coated with copper foam (upper) (* corresponds to the (111) peak of the underlying Al substrate), (b) an uncoated polycrystalline copper substrate.

(fcc) with high crystallinity and peaks corresponding to the (111), (200), and (220) crystal facets. The ratios of different pairs of crystal facets for the copper foam electrode are 1.24 for (111):(200), 3.6 for (111):(220), and 2.9 for (200):(220). For comparison, the XRD of a polycrystalline copper substrate is shown in Figure 2b, which also exhibits the (111), (200), and (220) crystal facets. The ratios of different pairs of crystal facets are 1.61 for (111):(200), 3.7 for (111):(220), and 2.3 for (200):(220). Although identical facets are observed in both samples, the amount of (200) facet is ∼22% higher in the copper foams than in the smooth electrode (see Supporting Information). This difference may be significant enough to affect product distribution in the electrochemical reduction of CO_2.

Shown in Figure 3 are the faradaic efficiencies of the various products obtained from the electro-reduction of CO_2 at a
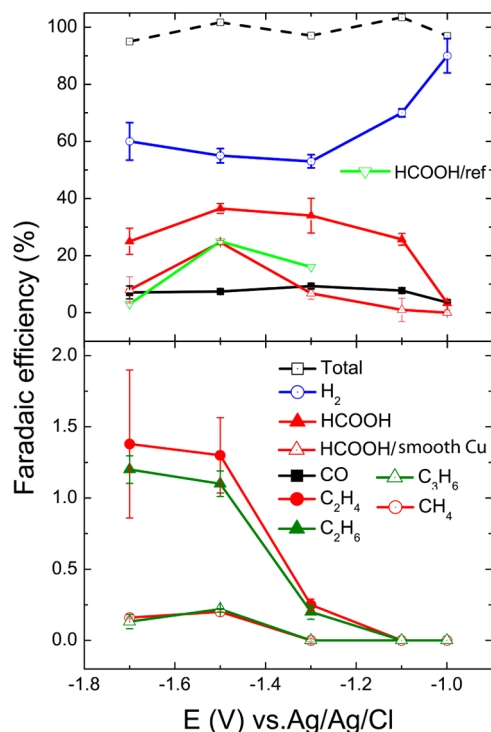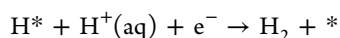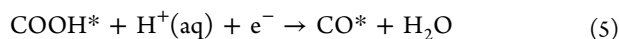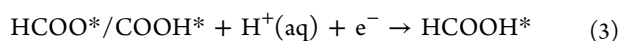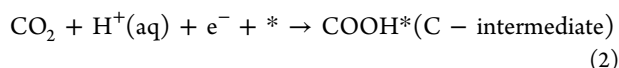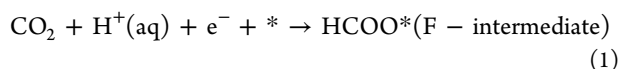

Figure 3. Product distribution as a function of applied potential during the electrochemical reduction of CO_2. The working electrode was a copper nanofoam electrodeposited for 15 s. Data for the electrochemical reduction of CO_2 to formate at a smooth copper electrode (both from our laboratory and from the literature) are included for comparison.

copper nanofoam (15 s electrodeposit) plotted as a function of applied voltage. The sum of the faradaic yield for all products approached 100% across the entire potential range. Major products were HCOOH, H_2, and CO, whereas minor products (<2%) were C_2H_4, C_2H_6, CH_4, and C_3H_6. Very small amounts of methanol and ethanol also were detected (≪1%) but were not quantified. The faradaic efficiency for HCOOH at a smooth copper electrode that was electro-polished prior to use was found to be similar (24% at −1.5 V) to that reported recently, where the same experimental conditions were used (i.e., smooth copper electrode produced HCOOH at a FE of 25% at −1.5 V in 0.1 M $KHCO_3$, pH 6.8).[15]

The onset potential for electro-reduction of CO_2 at copper foam electrodes was −1.0 V Ag/AgCl, at which the faradaic efficiency of HCOOH was 3−4%. This value increased to 26% at −1.1 V, which is significantly higher than that obtained at a smooth copper electrode (i.e., <1% at −1.1 V). In fact, the faradaic efficiency of HCOOH produced at copper foam electrodes was higher at all potentials with a maximum efficiency of 37% at −1.5 V, which is the highest value obtained for the electro-reduction of CO_2 to HCOOH at a copper electrode under ambient pressure. Furthermore, although the quantities of methane (CH_4) and ethylene (C_2H_4) generated were lower than those reported previously, ethane and propylene were generated in detectable quantities. Significantly, propylene has not been observed previously in the products of CO_2 electro-reduction at copper electrodes.

Experimental evidence that suggests the mechanism of CO_2 electroreduction is altered by the nanofoams comes from (*i*) increased faradaic efficiency for formate at all potentials, (*ii*) decreased faradaic efficiency for CO, CH_4, and C_2H_4, (*iii*) production of saturated hydrocarbons, namely, C_2H_6, and (*iv*) generation of novel C3 products, namely, C_3H_6. Insight into the significance of (*i*)−(*iii*) is provided by the detailed theoretical description of the chemical processes that occur at the copper−water interface during electrochemical reduction of CO_2 by Norskov et al.[21,22] In their studies, the electrochemical reaction was simulated using the computational hydrogen electrode (CHE) model coupled with adsorption energies of various reduction intermediates obtained from density functional theory (DFT) calculations. Voltage-dependent pathways for CO_2 reduction at copper surfaces were predicted: the formate (OCHO) or F-intermediate pathway, which leads exclusively to formic acid, or the carboxyl (COOH) or C-intermediate pathway, a branched pathway that leads to formic acid and higher-order hydrocarbons. Calculations for both pathways were performed on (111), (100), and (211) surfaces of copper. On the basis of these calculations and available experimental evidence, the electrochemical reduction of CO_2 at copper is predicted to proceed through a series of steps (1−6). The competing hydrogen evolution reaction proceeds through two steps (7 and 8). The asterisk (*) in any step denotes either a surface-bound species or a vacant, catalytically active site.

On (111) and (100) surfaces, the F-intermediate pathway dominates, because it has the lowest change in free energy of the two pathways.[21] Assuming (100) and (200) surfaces to be equivalent in DFT calculations, production of HCOOH via the F-intermediate pathway (steps 1 to 3 to 4) is expected to be enhanced at Cu nanofoams, where 22% more (200) surface is observed (cf. Figure 2 and Supporting Information).

$$CO_2 + H^+(aq) + e^- + * \rightarrow HCOO^*(F - \text{intermediate}) \tag{1}$$

$$CO_2 + H^+(aq) + e^- + * \rightarrow COOH^*(C - \text{intermediate}) \tag{2}$$

$$HCOO^*/COOH^* + H^+(aq) + e^- \rightarrow HCOOH^* \tag{3}$$

$$HCOOH^* \rightarrow HCOOH + * \tag{4}$$

$$COOH^* + H^+(aq) + e^- \rightarrow CO^* + H_2O \tag{5}$$

$$CO^* + H^+(aq) + e^- \rightarrow CHO^* \tag{6}$$

$$H^+(aq) + e^- + * \rightarrow H^* \tag{7}$$

or

$$H^* + H^+(aq) + e^- \rightarrow H_2 + * $$

$$H^* + H^* \rightarrow H_2 + 2* \tag{8}$$
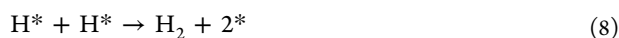
The free energy diagrams provided by DFT calculations also indicate that production of HCOOH at the (211) surface should be favored over (111) and (100) surfaces. Although the (211) surface is not observed experimentally, it can be used to model defects such as surface steps, which are found on rough surfaces. Experimental evidence in support of this prediction can be obtained by measuring the faradaic efficiency of HCOOH generated at Cu nanofoams of increasing thickness (and therefore, increasing total area of rough or highly stepped surfaces). The relative increase in surface area of copper foams

electrodeposited for different amounts of time was measured by analyzing voltammetric and SEM data, which are provided in Supporting Information. Shown in Figure 4a is the product
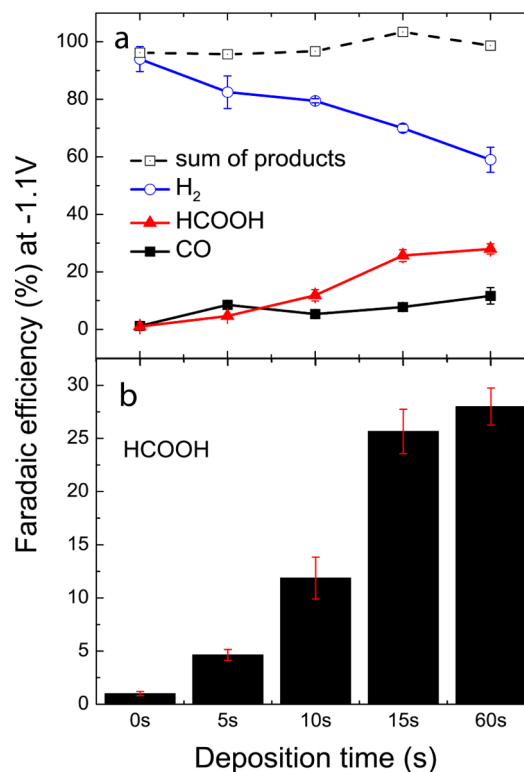

Figure 4. (a) Distribution of products from electro-reduction of CO_2 at copper electrodes coated with different amounts of copper foam (represented by their electrodeposition time). (b) Faradaic yield of HCOOH as a function of the copper foam used (represented by its electrodeposition time).

distribution obtained from the electrochemical reduction of CO_2 at different copper foams using an applied potential of only −1.1 V where H_2, HCOOH, and CO are the major products. Highlighted in Figure 4b is the faradaic efficiency of HCOOH as a function of increasing thickness (and total area of stepped surface) of the copper nanofoams. The maximum value obtained was 29% using a copper nanofoam that was electrodeposited for 60 s. This value is one of the highest values reported at copper (with the exception of 33% at −1.1 V using a copper oxide surface).[16] This value, however, is not much higher than the faradaic efficiency obtained at copper nanofoams electrodeposited for shorter times (i.e., 26% at 15 s), suggesting the effect of surface roughness may taper as the nanofoams become thicker (i.e., electrodeposition times >60 s). Nevertheless, these results confirm theoretical predictions that surface roughness has a dominant role in the faradaic efficiency of HCOOH despite the 22% increase in the (100) surface in the copper nanofoams.

DFT calculations on (111), (100), and (211) surfaces of copper also indicate the (211) surface is more likely than (111) and (100) surfaces to be involved in CO_2 activation and reduction to hydrocarbon products. Hydrocarbon production is predicted to occur via a branch in the C-intermediate pathway that goes through a CO* intermediate (steps 2 to 5 to 6).[22] This prediction was confirmed experimentally, where an increase in selectivity toward ethylene generation (14% vs

23% vs 37%) corresponded to copper electrodes of increasing roughness (electropolished < sputter coated < nanoparticle coated, respectively), while concurrently yielding very low amounts of HCOOH (i.e., <8%).[18] Comparing these results to those obtained with copper nanofoams indicates (1) surface roughness alone does not account for the high faradaic efficiencies for HCOOH production at copper nanofoams and (2) the branch of the C-intermediate pathway that goes through a CO* intermediate appears to be suppressed at copper nanofoams because very low faradaic efficiencies for CO (and its subsequent products, CH_4 and C_2H_4) are observed.

Finally, the generation of novel C3-products such as propylene (observation *iv*) may be caused by the hierarchical porous nature of the copper foams. Increasing the electro-deposition time results in an increase in the thickness of the copper foam (and depth of "channels") with a simultaneous increase in the pore diameter as the distance from the substrate increases. Thus, a gradient of pore diameters exists in the foam structure, which yields labyrinthine channels with conical-like shapes where the tip of the cone occurs at the underlying copper substrate. Within these channels are nanoscale dendritic features surrounded by nanoscale cavities of electrolyte. Consequently, the residence times of various intermediates within these confined volumes may increase, allowing for the production of products not observed at a smooth Cu electrode (i.e., propylene). The idea that nanoporous electrodes facilitate reaction pathways that are different from those that occur at smooth electrodes via a confinement mechanism has been studied in the electro-reduction of O_2 at nanoporous Pt electrodes.[26,27] This mechanism is based on the fact that within a nanopore, the electrical double layer (EDL) will overlap, thereby overlapping the corresponding electric field. Over-lapping EDL occurs easily in nanoporous structures because the thickness of the EDL is considerably larger than the volume within the pores. Even when a high overpotential is applied, the inner surface area of the pore is not accessible.

Gouy−Chapman theory[26] relates the Debye length of the EDL to electrolyte concentration, where the thickness of the EDL decreases as the concentration of the electrolyte increases. At a critical concentration of electrolyte, the EDL becomes sufficiently thin such that electric field of adjacent pores no longer overlap. Instead, the electric field maps the exact shape of the pores, thereby providing additional surface area to participate in the electrochemical reaction. Chronoampero-metric experiments (Figure 5) reveal that the current density at a smooth copper electrode increases gradually from 7 to 31 mA/cm^2 (∼4.5X) as the electrolyte concentration increases from 0.1 to 1 M. In contrast, the current density at a copper nanofoam (60 s sample) increases steeply from 10 to 82 mA/cm^2 (∼8X) above a critical concentration of 0.5 M $KHCO_3$. It is evident from this data that nanoscale pores are present within the copper foam electrodes, which become accessible only at concentrations above 0.5 M $KHCO_3$ (i.e., where the thickness of the double-layer is minimized and does not overlap within a three-dimensional nanopore or channel). These three-dimensional electroactive areas, if small enough, could reduce the kinetics of desorption of surface intermediates and con-sequently enable the production of C2 or C3 products such as propylene by increasing the residence time of surface intermediates. Unfortunately, the proton reduction reaction becomes more favorable above this critical concentration.

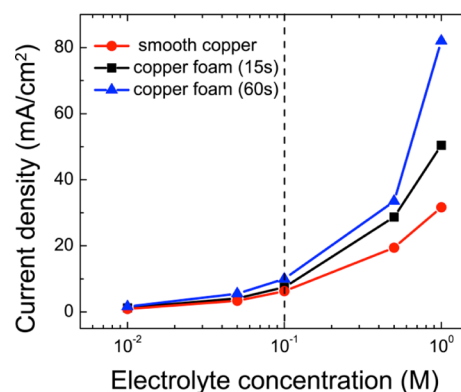The results presented herein demonstrate that the electro-reduction of CO_2 at copper nanofoams differs from that

Figure 5. Chronoamperometric data of CO_2 electro-reduction at smooth and copper foam electrodes plotted as a function of electrolyte concentration, where the electrolyte was $KHCO_3$ saturated with CO_2 and the step potential was −1.8 V. The dashed line corresponds to the electrolyte concentration used for all electrolysis experiments performed in this study, where the step potential varied between −1.0 and −1.8 V.

observed at smooth copper electrodes with respect to the onset potential, products formed, and their potential dependent distribution. Products from the electro-reduction of CO_2 were observed at −1.0 V, indicating an onset potential that is ∼200 mV more positive than that required at smooth copper electrodes. This decrease in overpotential may be a consequence of the higher (200) surface orientation in the copper nanofoams (by 22%) compared to smooth copper. Furthermore, the electro-reduction of CO_2 at copper nano-foams at different potentials yielded a significantly different product distribution compared to that at smooth copper (most notably, the faradaic efficiency of formate was 26% at −1.1 V compared to only 3% at smooth copper). The enhanced faradaic efficiency of HCOOH, the decreased faradaic efficiency of methane and ethylene, and the presence of ethane and propylene (not observed at smooth copper) at copper nanofoams suggest that the electro-reduction of CO_2 follows both the F-intermediate and C-intermediate pathways, with the C-intermediate pathway to HCOOH becoming more dominant as the thickness (and total amount of stepped surface) of the copper nanofoam increases. Systematically increasing the thickness of the copper nanofoams further enhances the faradaic efficiency of HCOOH up to 29% by suppressing the electrochemical reduction of adsorbed H* to H_2. Finally, evidence is provided that some areas within the copper nanofoams only become electrochemically accessible above a critical concentration of electrolyte.

In summary, the copper nanofoams used in this study reveal that novel electrode architectures offer another approach to affecting the products formed during the electrochemical reduction of CO_2. Studies that examine how systematic changes in pore diameter, pore depth, and electrolyte concentration affect the products obtained from the electro-chemical reduction of CO_2 are ongoing and will be reported elsewhere.

■ ASSOCIATED CONTENT

Ⓢ Supporting Information

Includes experimental methods, measurements of electroactive area, and voltammetric analysis. This material is available free of charge via the Internet at http://pubs.acs.org.

■ AUTHOR INFORMATION

Corresponding Author
*E-mail: Tayhas_Palmore@brown.edu.

Notes
The authors declare no competing financial interest.

■ ACKNOWLEDGMENTS

■ REFERENCES

(1) Hori, Y.; Murata, A.; Kikuchi, K.; Suzuki, S. *J. Chem. Soc., Chem. Commun.* **1987**, 728−729.
(2) Hoshi, N.; Kawatani, S.; Kudo, M.; Hori, Y. *J. Electroanal. Chem.* **1999**, *467*, 67−73.
(3) Hori, Y.; Murata, A.; Takahashi, R. *J. Chem. Soc., Faraday Trans.1* **1989**, *85*, 2309−2326.
(4) Hori, Y.; Murata, A. *Electrochim. Acta* **1990**, *35*, 1777−1780.
(5) Tomita, Y.; Hori, Y. *Stud. Surf. Sci. Catal.* **1998**, *114*, 581−584.
(6) Jhong, H.-R. M.; Ma, S.; Kenis, P. J. A. *Curr. Opin. Chem. Eng.* **2013**, *2*, 191−199.
(7) Gattrell, M.; Gupta, N.; Co, A. *J. Electroanal. Chem.* **2006**, *594*, 1−19.
(8) Hori, Y. In *Modern Aspects of Electrochemistry*; Vayenas, C., White, R., Gamboa-Aldeco, M., Eds.; Springer: New York, 2008; Vol. *42*, pp 89−189.
(9) Ohta, K.; Kawamoto, M.; Mizuno, T.; Lowy, D. A. *J. Appl. Electrochem.* **1998**, *28*, 717−724.
(10) Hori, Y.; Konishi, H.; Futamura, T.; Murata, A.; Koga, O.; Sakurai, H.; Oguma, K. *Electrochim. Acta* **2005**, *50*, 5354−5369.
(11) Hori, Y.; Murata, A.; Takahashi, R.; Suzuki, S. *J. Chem. Soc., Chem. Commun.* **1988**, 17−19.
(12) Hori, Y.; Takahashi, I.; Koga, O.; Hoshi, N. *J. Phys. Chem. B* **2002**, *106*, 15−17.
(13) Hori, Y.; Takahashi, R.; Yoshinami, Y.; Murata, A. *J. Phys. Chem. B* **1997**, *101*, 7075−7081.
(14) Hori, Y.; Wakebe, H.; Tsukamoto, T.; Koga, O. *Electrochim. Acta* **1994**, *39*, 1833−1839.
(15) Kuhl, K. P.; Cave, E. R.; Abram, D. N.; Jaramillo, T. F. *Energy Environ. Sci.* **2012**, *5*, 7050−7059.
(16) Li, C. W.; Kanan, M. W. *J. Am. Chem. Soc.* **2012**, *134*, 7231−7234.
(17) Schouten, K. J. P.; Kwon, Y.; van der Ham, C. J. M.; Qin, Z.; Koper, M. T. M. *Chem. Sci.* **2011**, *2*, 1902−1909.
(18) Tang, W.; Peterson, A. A.; Varela, A. S.; Jovanov, Z. P.; Bech, L.; Durand, W. J.; Dahl, S.; Norskov, J. K.; Chorkendorff, I. *Phys. Chem. Chem. Phys.* **2012**, *14*, 76−81.
(19) Reske, R.; Mistry, H.; Behafarid, F.; Cuenya, B. R.; Strasser, P. *J. Am. Chem. Soc.* **2014**, *136*, 6978−6986.
(20) Lu, Q.; Rosen, J.; Zhou, Y.; Hutchings, G. S.; Kimmel, Y. C.; Chen, J. G.; Jiao, F. *Nat. Commun.* **2014**, *5*, 3242−3248.
(21) Durand, W. J.; Peterson, A. A.; Studt, F.; Abild-Pedersen, F.; Nørskov, J. K. *Surf. Sci.* **2011**, *605*, 1354−1359.
(22) Peterson, A. A.; Abild-Pedersen, F.; Studt, F.; Rossmeisl, J.; Norskov, J. K. *Energy Environ. Sci.* **2010**, *3*, 1311−1315.
(23) Hansen, H. A.; Varley, J. B.; Peterson, A. A.; Nørskov, J. K. *J. Phys. Chem. Lett.* **2013**, *4*, 388−392.
(24) Peterson, A. A.; Nørskov, J. K. *J. Phys. Chem. Lett.* **2012**, *3*, 251−258.
(25) Shin, H. C.; Dong, J.; Liu, M. *Adv. Mater.* **2003**, *15*, 1610−1614.
(26) Boo, H.; Park, S.; Ku, B.; Kim, Y.; Park, J. H.; Kim, H. C.; Chung, T. D. *J. Am. Chem. Soc.* **2004**, *126*, 4524−4525.
(27) Bae, J. H.; Han, J.-H.; Chung, T. D. *Phys. Chem. Chem. Phys.* **2012**, *14*, 448−463.